Heliyon 7 (2021) e07680

Contents lists available at ScienceDirect

Heliyon

journal homepage: www.cell.com/heliyon

Research article

Refraction seismic complementing electrical method in subsurface characterization for tunneling in soft pyroclastic, (a case study)

Shimeles Fisseha [a,*], Getnet Mewa [a], Tigistu Haile [b]

[a] IGSSA, Addis Ababa University, P. O. Box 1176, Addis Ababa, Ethiopia
[b] SES, Addis Ababa University, P. O. Box 1176, Addis Ababa, Ethiopia

ARTICLE INFO

Keywords:
Integrated approach
Refraction seismic
DC resistivity
Subsurface characterization
Main Ethiopian Rift (MER)

ABSTRACT

The paper highlights the potential drawback of mapping a single geophysical property for subsurface characterization in potential engineering sites. As an exemplary case study, we present the geophysical survey conducted along the surface projection of a tunnel in the quaternary volcanic terrain of the Main Ethiopia Rift. Initially, geoelectrical mapping involving 12 Vertical Electrical Sounding (VES) and a short Electrical Resistivity Imaging (ERI) line, was carried out. The 1D geoelectric model indicates that the formation resistivity at tunnel zone varies from 50 to 500 Ω·m. The corresponding value on 2D model, (>350 Ω·m), is also compatible. Based on limited available geological information, the geoelectric horizon was attributed to weathered and variably saturated ignimbrite. Following unexpected encounter during excavation, refraction seismic and core drilling were carried out for additional insights. Tomographic analysis of the seismic arrival times revealed that below a depth of 45 m, (tunnel zone), the velocity substratum is marked by a range, (1200–1800 m/s). Such low velocity range is typical of unconsolidated materials and, thus, cannot rationalize the geoelectrical attribution (ignimbrite). In a joint interpretation, the likely formation that may justify the observed range of the electrical resistivity and low P-wave velocity appears to be unwelded pyroclastic deposit (volcanic ash). Eventually, core samples from the tunnel zone confirmed the presence of thick ash flow. However, the unexpected ground conditions encountered at the early phase, due to insufficient information derived from a single geophysical parameter, caused extra cost and considerable delay.

1. Introduction

The role of geophysical methods in supporting engineering site characterization is becoming progressively popular. DC Electrical Resistivity and Refraction Seismic are the most popular geophysical methods in engineering site assessments. This is due to the fact that spatial distribution of the electrical resistivity and longitudinal wave velocity of subsurface materials are closely related, among other factors, to porosity and fluid content, (Meju et al., 2003; Carcione et al., 2007; De Pasquale et al., 2019).

Owing to the inherent ambiguity in the interpretations of geophysical models, integrating more than one method is an indispensable guideline devised to reduce geological uncertainty, Telford et al. (1990). This is particularly important in engineering site assessments. The huge variations in the measurable physical properties (by many orders of magnitude), the wide range of overlap and spatial heterogeneity in near-surface material makes geological interpretations quite arbitrary. Moreover, each geophysical method has certain advantages and limitations, (e.g., Varnavina et al., 2019; Pazzi et al., 2019). However, there are certain cases in which geophysicists are contended to reduce volume of work or urged to use only one geophysical technique for the purpose of cost minimization.

The subject of this paper is to highlight the potential drawback of studying a single petro-physical parameter for characterizing subsurface materials in engineering site assessments. The case study also demonstrates the advantage of combining refraction seismic and geoelectrical observations, as complementary tools, for evaluating soft volcanic terrain such as pyroclastic deposits for engineering designs.

This study is related to a gravity-based surface irrigation project in Dodota district, Central Ethiopia. The project is designed to irrigate over 1,100 ha of less productive, predominantly rain fed land by drawing water from Keleta River. Its full implementation involves constructing a 78 m weir, a water conveying tunnel, and a diversion structures (12.4 km primary canal and 9.5 km secondary and tertiary canals). The tunnel,

* Corresponding author.
E-mail addresses: shimeles.fisseha@aau.edu.et, wmikel99@gmail.com (S. Fisseha).

https://doi.org/10.1016/j.heliyon.2021.e07680
Received 15 June 2020; Received in revised form 30 September 2020; Accepted 26 July 2021

which is the focus of this manuscript, is envisaged to convey water from a weir across the Keleta River to a floodplain River Boru, which feeds the canals in the irrigable area. The tunnel alignment spans about 2 km in the northwest direction from the intake (543631.00 m E, 910406 m N), left side of the Keleta River, to the outlet (542422.00 m E, 912270 m N). The ground elevation along the proposed alignment is in the range of 1658 m–1730 m [a. s. l.].

The project area is located near the Sire border fault systems (Figure 1a) on the eastern margin of the Northern Main Ethiopian Rift (NMER). The region is characterized by active extensional tectonics (e.g., Bonini et al., 2005; Corti, 2009; Corti et al., 2018). The study site falls on the geological map of the Nazret-Dera region, specifically on the Dhera-Sodere-Nazareth lithological group, (Alula et al., 1992). According to the geological map of the study area, the dam site and the surrounding area is generally overlain by a sequence of unwelded ignimbrites forming the flat plains west of the Keleta River. This surface unit is underlain by a thick sequence of vari-coloured and variably welded ignimbrite layers intercalated with basalt and palaeosol layers. These are seen exposed across the gorges of the Keleta and Boru Rivers. At deeper levels, the rock unit is composed of coarse-grained, loosely welded ignimbrite intercalated with basalts and trachy basalts. Basaltic agglomerates are also present, (Figure 1b).

In the active sectors of the Main Ethiopian Rift, the design of subterranean structures require careful geotechnical considerations. This is because, the terrain characteristics, the underlying multifaceted geology and the tectono-magmatic activity (Biggs et al., 2011; Agostini et al., 2011; Corti et al., 2020) could be detrimental to the viability and sustainability of subsurface engineering structures.

The geophysical work presented in this paper was purposed to map the variations in physical parameters of the ground mass beneath the tunnel alignment. Ostensibly for cost reduction, the subsurface was initially mapped using a single geophysical technique, Direct Current (DC) electrical resistivity method. The resistivity survey involved twelve (12) Vertical Electrical Soundings (VES) points and about 440 m long Electrical Resistivity Imaging (ERI). Using the results of quantitative analysis of the VES curves, the subsurface resistivity stratification was established as a geoelectric section. Then, based on lithological log data from nearby boreholes, the subsurface geoelectric horizon corresponding to the tunnel zone was interpreted to denote a fractured and variably saturated ignimbrite. The result on geoelectric survey was then communicated cautiously with strong recommendations for additional studies. Regardless of the caveats, a design was made and earth work was started. However, the geologic materials encountered during the early excavation was different from what were referred in the design document. Then, realizing the need for further information on the ground conditions, refraction seismic survey and rotary core drillings were conducted along the geoelectric survey line. The additional insight obtained from the compressional wave velocity proves very useful in dictating the interpretation of the geoelectric models. The joint appraisal was, subsequently, validated by the lithological log of samples cored from the tunnel zone. However, the unexpected ground conditions encountered at the early phase resulted in considerable delay and incurred extra cos. This was, essentially, due to insufficient information derived from a single geophysical parameter.

The main purpose of this paper is, therefore, sharing this experience as a typical example of wrong judgment and malpractice. The findings also emphasize the indispensability of integrated approach in near-surface applications of geophysical methods.

In the next sections, the method applied in the study are given in detail and supported by the literature. In the result section, we present

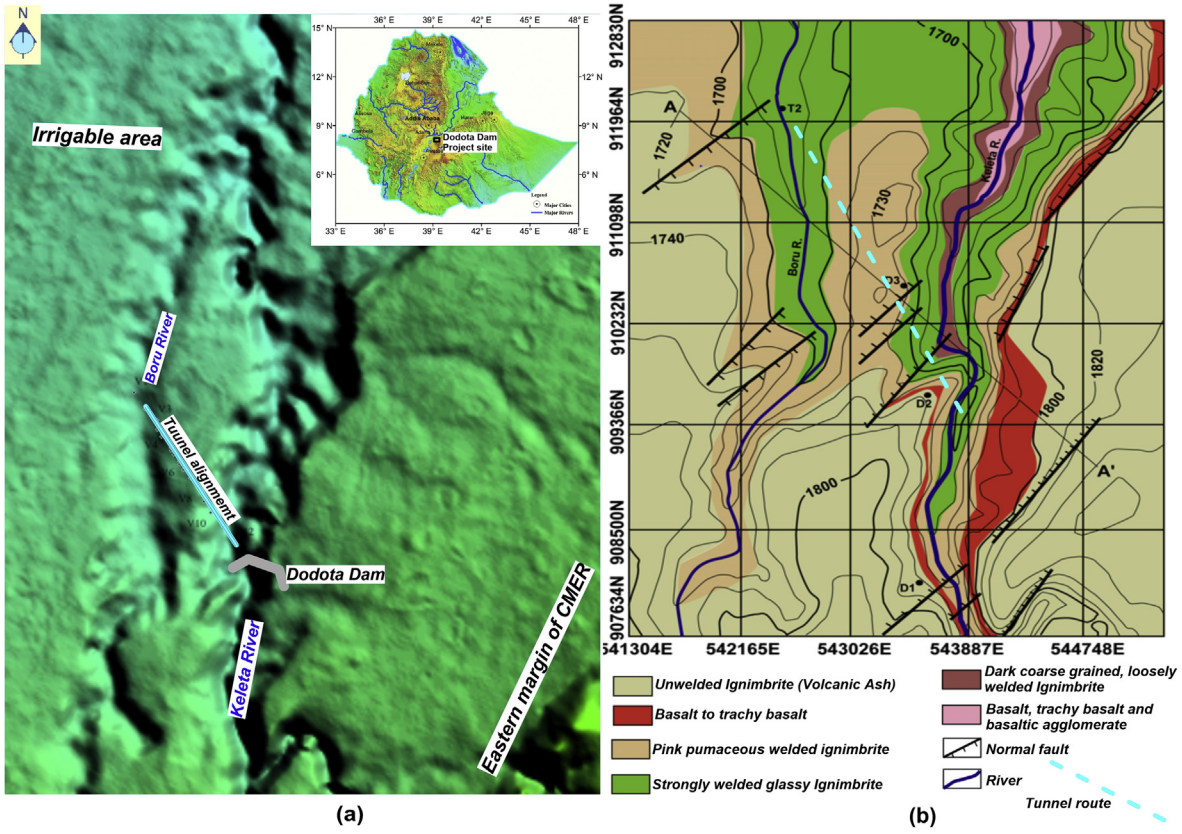

Figure 1. Location and geology of the study area. a) The main morphological features and major engineering structures of the Dodota dam site shown on digital elevation model (Shuttle Radar Topography Mission data from https://topex.ucsd.edu/cgi-bin/get_srtm30.cgi, Becker et al., 2009). b) The geological map of the study area (modified from Geology of Dodota irrigation project site, Integrated Geophysical and Geological site assessment for Dodota Dam project, 2015, unpublished technical report).

and discuss the main findings of the geoelectrical survey and its interpretations. Then, we present the P-wave velocity model and the joint consideration for the geological appraisal. Finally, we conclude by summarizing and substantiating the salient features of the work.

2. Material and methods

2.1. Data acquisition and processing

The schematic diagram on Figure 2 shows the relative positions of the geophysical survey lines along the elevation profile of the tunnel alignment. The DC Electrical Resistivity (1D - Sounding and 2D - Imaging) and Refraction Seismic data considered in this paper is part of the geophysical data set acquired between 2015 and 2018, to characterize the subsurface geology.

2.1.1. DC electrical resistivity survey

2.1.1.1. VES. The instrument used for the DC Electrical resistivity survey was a SYSCAL R1-Plus Switch 72 unit of IRIS Instruments (with full accessory and other ancillary materials). The Vertical Electrical Sounding (VES) measurement was done at twelve points using the Schlumberger electrode array and maximum current electrode separation of AB/2 = 330m. The average separation between VES points was about 200m. An initial insight on the geoelectrical behavior of the subsurface was obtained from the pseudo-depth sections plot. The plot gives a display of both horizontal and vertical variations in apparent resistivity simultaneously. In the present analysis, instead of the routine current electrode separation (AB/2), effective depth (Edwards, 1977) surface is used for plotting the pseudo sections from the topographic surface. Detailed quantitative analysis and 1-D forward modelling and inversion of VES data was done using WinRESIST (Vander Velpen, 2004). Starting from an initial model, the optimal number of layers and the corresponding parameters, the software performs inversions to determine the optimal thicknesses, and 'true' resistivities of the subsurface layers.

2.1.1.2. ERT. For the multi-electrode - 2D resistivity data, we used the Iris SYSCAL R1 Plus Switch instrument working in "multi-electrode mode" in Wenner-Schlumberger configuration. This is an array with the longest outer electrode separation and provides a relative advantage of wider coverage and deeper penetration of about 68m (e.g., Dahlin and Zhou, 2004). With 72 electrodes connected to a 360m long cable (with 5m electrode spacing), we used one roll-along leeway to extend the profile to 440m. The actual position of the ERT profile is about 120 m to the northeast of the surface projection of the tunnel alignment where the VES and refraction seismic lines are collocated. The electrical resistivity tomography data was appraised using a 2D processing software, RES2DINV (Loke, 2002). Based on the smoothness constrained least-squares method (De Groot-Hedlin and Constable, 1990; Loke and Barker, 1996), the software package determines a two dimensional (2D) resistivity model of the subsurface that fits the measured apparent resistivity data with minimum root-mean squared (RMS) error. The 2D inversion of the current ERI data was done using the topographic modelling option to account for altitude variation along the survey line.

2.1.2. Refraction seismic

The seismic refraction survey was carried out using the DOLANG Seismograph (JEA247ESAC 500) with 10 Hz vertical geophones and sets of 12-channel spread cables. The P-wave energy was generated using a 12Kg impact hammer (Sledge Hammer) on a striking plate. The acquisition software allows using such features as zooming, filtering, time stretching, Automatic Gain Control (AGC) and balancing of traces. Gain levels were adjusted with setting the inbuilt amplifier so as to minimize noise created by ambient sources. All possible signal enhancement techniques were also used. The Seismic refraction data was acquired over 5 spreads, i.e. one 36 and the other four 24 channels and saved in SEG2 format. With the 10 m geophone spacing, the length of the spreads is 230 m and 350 m for the 24- and 36-channel, respectively. Each spread was measured independently with two overlapping geophones resulting in a continuous profile covering about 1230 m distance along the tunnel route.

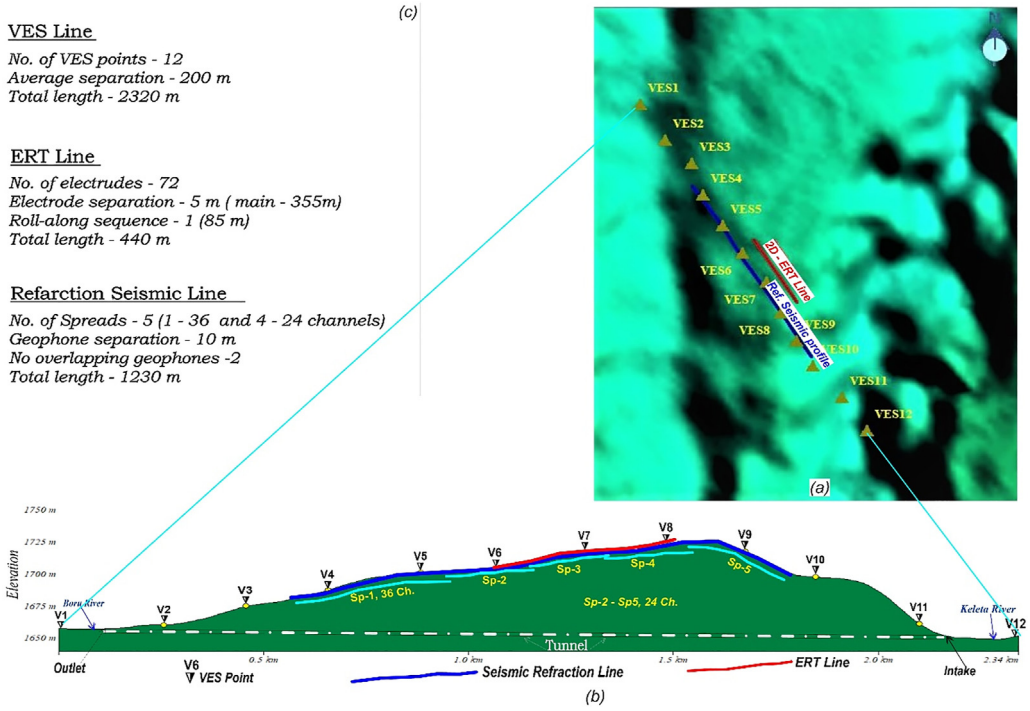

Figure 2. Location map of the study area. a) The plan view of the tunnel alignment on shown on digital elevation model (Shuttle Radar Topography Mission data from https://topex.ucsd.edu/cgi-bin/get_srtm30.cgi, Becker et al., 2009). b) Topographic profile along the surface projection of the tunnel alignment showing the relative positions of the geophysical survey lines and points. c) A panel showing geophysical survey specifications and volume of data.

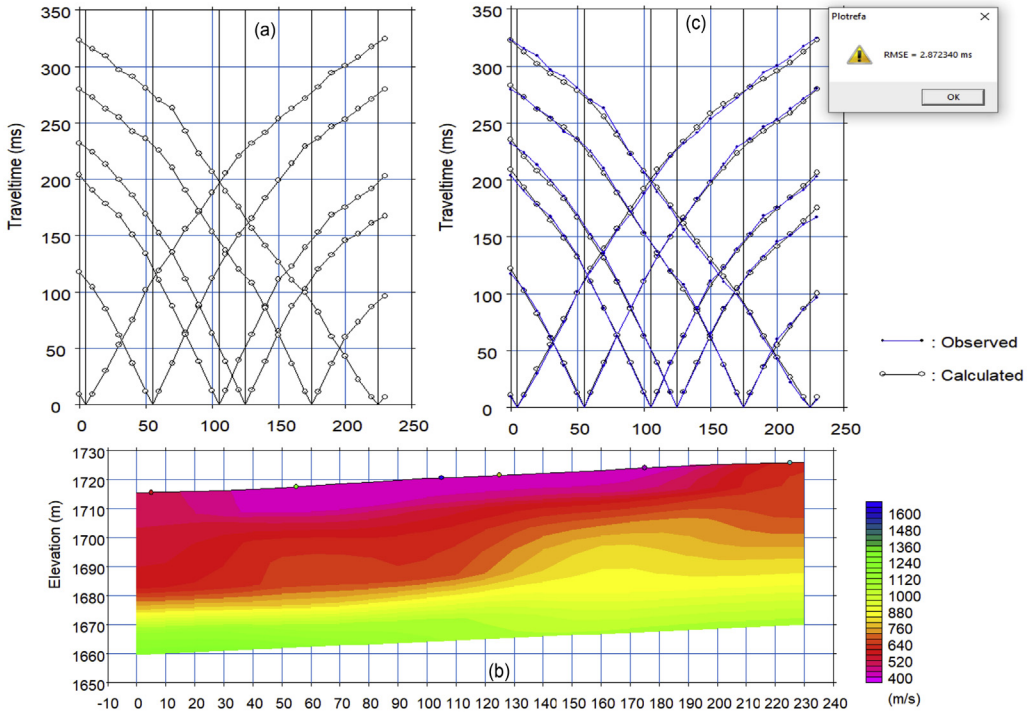

Figure 3. The input data, the time –distance graph of the first arrivals (a), the p-wave velocity tomogram (b) and a graph showing the fit between the measured and theoretical travel time of the tomography model (c) of central profile along the tunnel route, Spread-3.

The refraction seismic data analysis was done using SeisImager/2D - a multi-component, 2D seismic refraction software. First, *PickWin95* was used for routine wave processing and picking first breaks of the P-wave. After loading the field data (in SEG2-formats), the first breaks are marked automatically on the mean normalized waveform. Then, after applying amplitude gain to enhance the visibility of the weak signal on traces, the first arrivals were picked manually. The first arrivals from all shots were saved in a travel-time data file for further analysis.

The second software – "PlotRefa" was then used to analyze the first arrival times picked by *PickWin95*. The input is the time-distance data-a file containing first arrival times from multiple shots of a geophone spread (and optionally, elevation data). Initially, velocity models were obtained using the Time-term inversion, assuming uniform vertical stratification. The outputs were then used as inputs (starting models) for final refinement through tomographic inversion. During tomographic inversion, the parameters in the starting model modifies iteratively, reducing the discrepancy between the computed travel time (model response) and the measured field data. When the inversion converges, i.e., when further iterations cease to reduce the root-mean-square (RMS) error, the process terminates and the parameters of the last iteration constitute the final model.

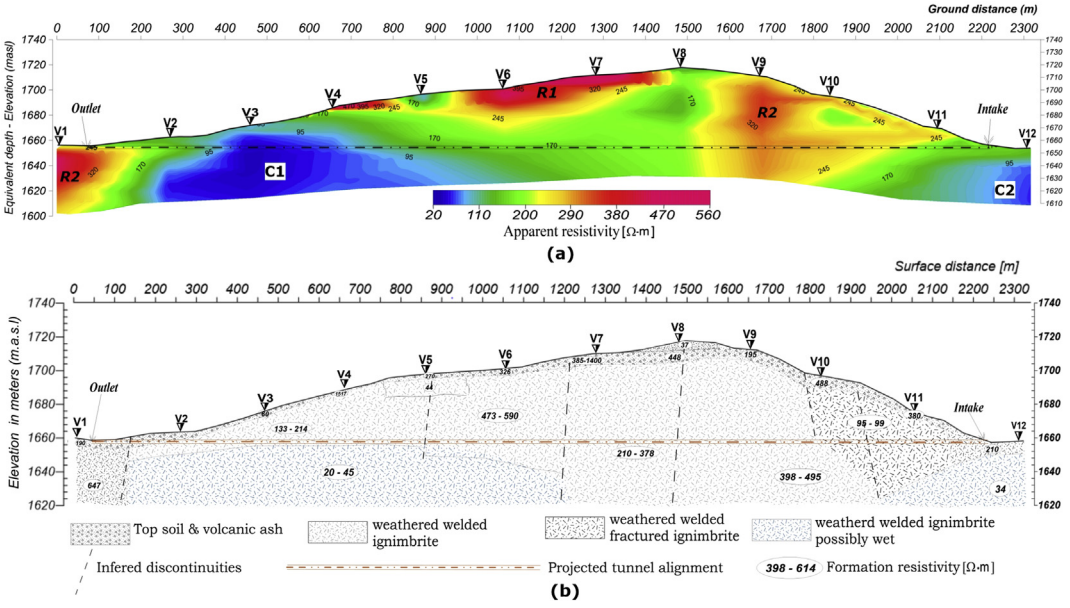

Figure 4. The subsurface geoelectrical picture along the tunnel alignment. (a) Apparent resistivity pseudo-depth section and (b) interpreted geoelectric section constructed based on the inverted model parameters.

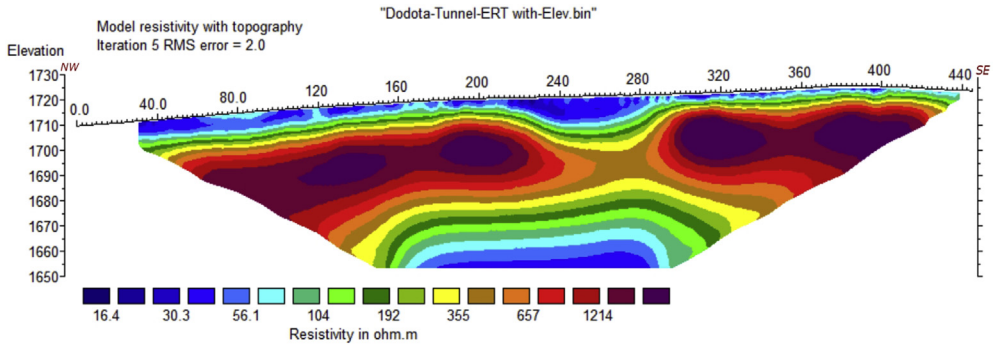

Figure 5. The model section obtained from the 2D inversion of the electrical resistivity imaging data along a short line in the middle of the tunnel alignment.

PlotRefa avails various options, including tomographic inversion which provides the image of the subsurface velocity model automatically. Figure 3 displays one such final model from the present study in a typical PlotRefa graphics.

For each individual spread, the final model parameters was saved in a formatted text file (X, Z, V) with: X – geophone distance, Z – depth (elevation) and V- the corresponding P-wave Velocity. The final velocity tomogram is obtained by dovetailing the individual velocity model files.

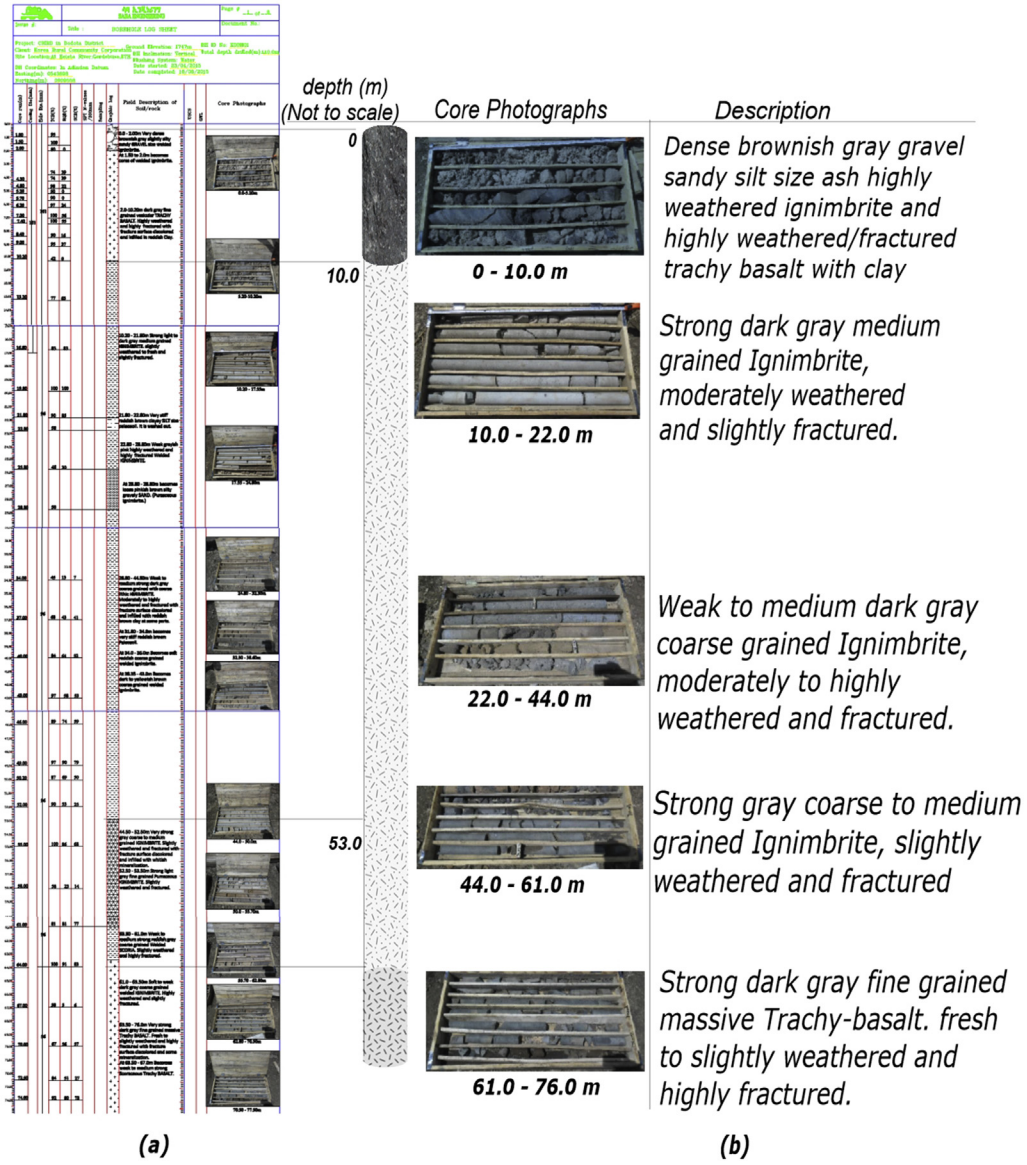

Figure 6. Images showing the log sheet of Borehole-KDBH01, drilled on left shoulder of the Keleta River, (extracted from the unpublished drilling report, SABA ENGINEERING PLC, 2015). Original image from the report (a) and selectively enlarged boxes for visual clarity (b).

Starting from the first geophone (0-mark on spread-1), the X-values in spread-2 were increased from the end of spread-1 and so do subsequent spreads. The resulting file contains velocity-depth/elevation data along a continuous, 1230 m long, profile of the tunnel route.

3. Results and discussions

3.1. DC electrical resistivity

3.1.1. VES

The pseudo depth section, (Figure 4a), shows that the subsurface beneath the tunnel alignment is characterized by notable electrical heterogeneity with large variation in the measured apparent resistivity, ranging from <20 to >500 Ω·m.

In qualitative terms, there appears to be five distinct zones, three high and two low anomalous resistivity regions (Figure 4a). The first high apparent resistivity anomaly zone (R1) is delineated by values in excess of 350 Ω·m which typical of loose and dry materials. This shallow feature may mark out a soil horizon resulted from intensive weathering. The measured apparent resistivity in the other two moderately high response zones (R2) ranges between 250 and 350 Ω·m. Extending deeper into the subsurface, these two apparently resistive columns may indicate localized change in composition and/or texture. In contrast to R1 and R2, C1 and C2 are the two conductive horizons where the apparent resistivity values fall below 90 Ω·m. The drop in the measured electrical resistivity in the two low anomaly regions may suggests elevated water/moisture content or presence of other conductive constituents.

Referring to the geo-electric section, Figure 4b, the subsurface under the traverse line is represented by two to three geo-electric layers. On top, the layer with varying electrical resistivity and uneven thickness is thought to delineate the soil cover which is comprised of alluvium and residue from weathering of pyroclastic material. The thickness of the top layer undulates between 3 m and 7 m. Over the elevated portion, the soil horizon deepens to 20 m presumably reflecting the extent of weathering. The electrical resistivity in the top layer also exhibits a wide variation, ranging from <100 Ω·m to >1000 Ω·m. Over the large central portion, (between V4 and V10), the second layer is characterized by higher resistivity value (>300 Ω·m). However, towards both ends of the tunnel profile, the formation resistivity values drop below 200 Ω·m. The second geoelectric layer is interpreted to represent variably welded ignimbrite intercalated with thin basaltic layers and paleosoil. Except beneath the elevated central region, where the second layer persists to the bottom, a conductive (<60 Ω·m) appears as a geoelectric substratum. The likely reason for the drop in electrical resistivity could be elevated fluid/moisture content. The near-vertical discontinuities traced as boundaries between abrupt changes subsurface geoelectric signatures may indicate positions of possible structural features (weak zones) such as contacts or fractures.

3.1.2. ERT

The electrical resistivity values on the 2D model (Figure 5) range from 15 Ω·m to 1200 Ω·m. The conductive zone (<80 Ω·m) on top of the model section may represent the soil. The thickness of the soil mass increases from 3 m to 12 m down the slope to the northwest. However, around the central portion of the section, the conductive horizon forms a bowl shaped depression of 20 m deep. This probably indicates a fracture zone that cuts deeper through the underlying units. The vast intermediate portion of the section is characterized by resistivity values in excess of 600 Ω·m. This could be attributed to weathered and fractured volcanic unit, possibly welded tuff (ignimbrite). Between 240 m and 280 m marks, the resistive block appears bisected by a narrow, relatively conductive channel that may indicate fracture zone or other similar structure. Further down at a depth of about 50 m, the resistivity signature falls below 100 Ω·m. The plausible explanation for the reduction of electrical resistivity at deeper horizons could be increase in moisture content or water saturation. The resistivity stratification on the 2D model is broadly compatible to the 1D model.

The interpretation of the geoelectrical models was done assuming the continuity of the lithology sequence witnessed in boreholes located about 1 km SE of the tunnel intake. Two boreholes sunk on either side of the Keleta River encountered weathered and fractured ignimbrite at depths compatible with the tunnel zone. Figure 6 portraits images of the core boxes and descriptions of the lithological log of borehole-KDBH01. However, the material revealed during early excavation was loose material, dominantly, sand and silt size.

3.2. Seismic refraction

Figure 7 exhibits the plot of the P-wave velocity variation in the subsurface. In broader sense, the compressional wave velocity increases with depth. However, due to noticeable lateral variations, the boundaries between prominent seismic layers may not be easily discerned.

However, grouping the P-wave velocity values in discrete ranges, the subsurface can be segregated into three geoseismic layers. The top layer with a longitudinal wave velocity of 400–700 m/s is depicted by cold colors (bluish). This may represent the loose soil cover possibly produced

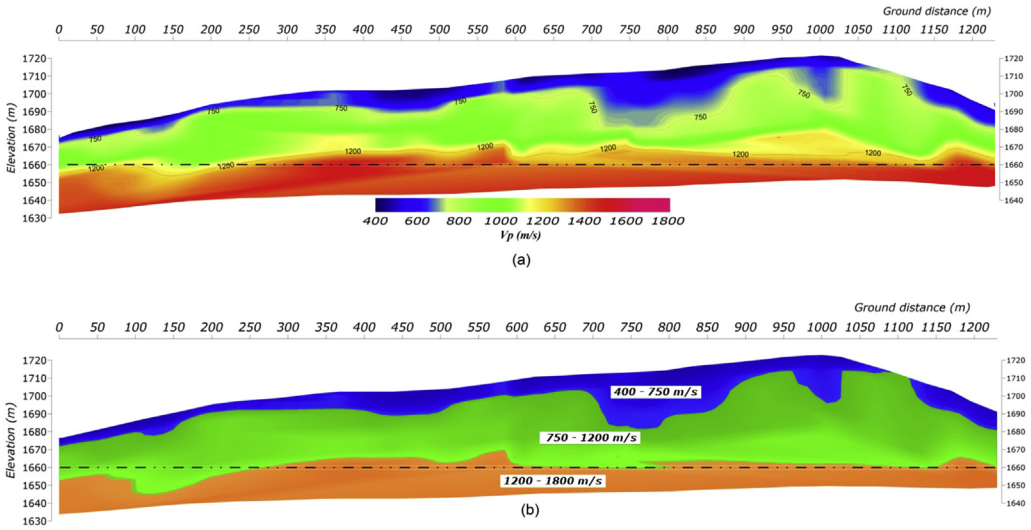

Figure 7. P-wave velocity section from the tomographic inversion results of refraction seismic data along the central portion of the tunnel alignment. The contoured plot of the P-wave velocity variation in the subsurface (a) and (b) the layered geoseismic models defined by finite ranges of the P-wave velocity.

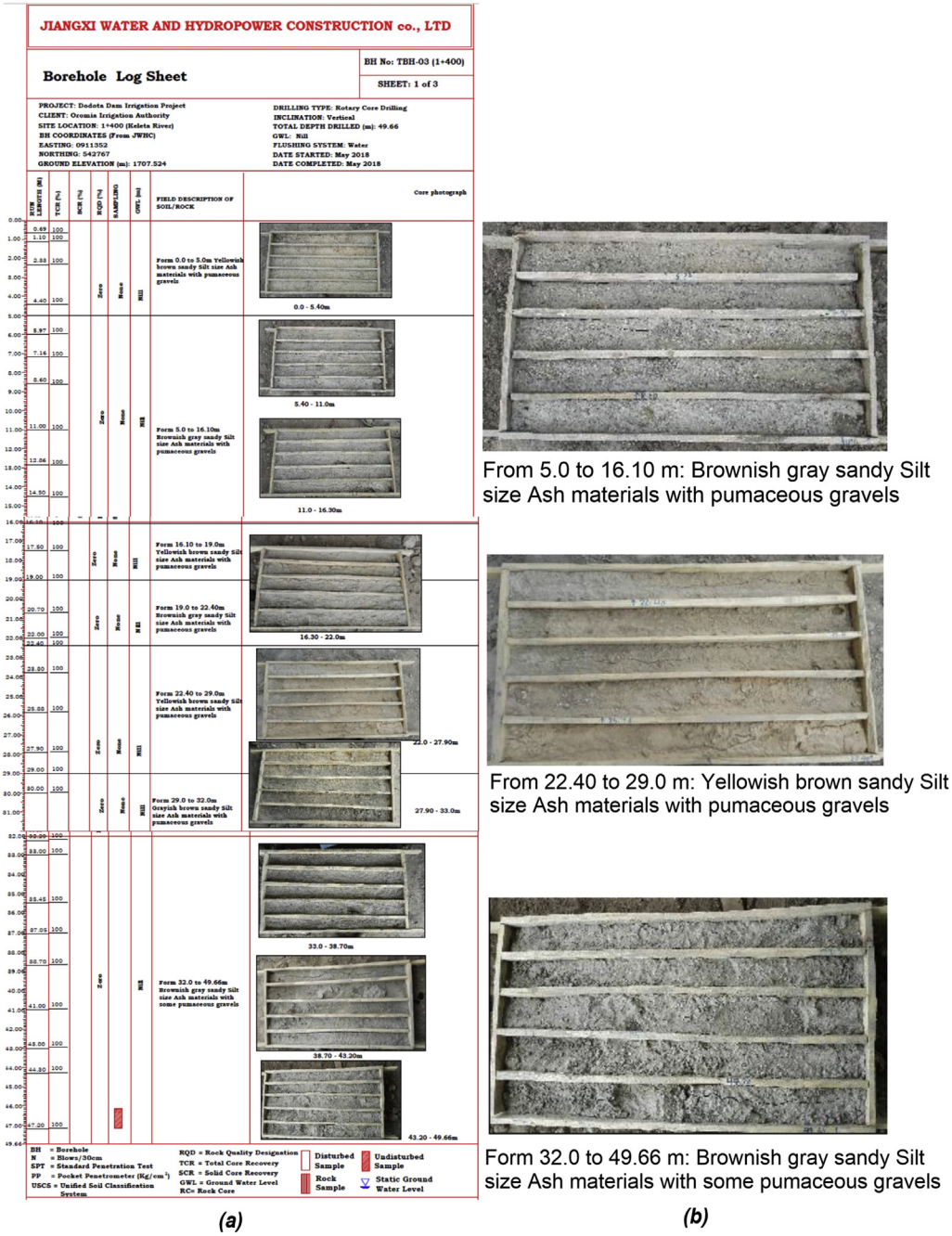

Figure 8. Images showing the log sheet from Borehole TBH03, drilled at the central part of the tunnel alignment, (extracted from the unpublished drilling report, JIANGXICO WATER AND HYDROPOWER CONSTRUCTION co. LTD, 2018). Original image from the report (a) and selectively enlarged boxes for visual clarity (b).

by weathering of pyroclastic materials. The thickness on the soil cover varies from 2 m to 7 m. However, between the ground marks of 720 m and 870 m, the soil thickness exceeds 20 m. With velocity ranging from 700 m/s – 1200 m/s, the subsurface horizon in the second (green layer) may represent loose material presumably, weathered and unwelded pyroclastic deposit. Finally, the transition to hot colors (reddish hue) at an average depth of 45–50 m from the ground surface, delineates the velocity substratum. This increment in longitudinal (P-wave) velocity from 1200 m/s to 1800 m/s may suggest gradual compaction of loose pyroclastic mass due to larger depth of burial. The other possible cause for a rise in P-wave velocity in loose/porous materials is increment in moisture/fluid content, usually water. Mavko et al. (2009) give a very good account of the dependence of seismic velocities on effective pressure and pore fluid.

Using field tomographic seismic velocity distributions and laboratory measurements on samples, Vinciguerra et al. (2006) studied the velocity properties of tuff and deduced that increasing hydrostatic pressure increases P- and S-wave velocities but strongly influenced by the geometry of the void space and the presence of pore fluids.

3.3. Joint appraisal of the geoseismic and geoelectric models

The seismic refraction model (Figure 7) shows that the overall compressional wave velocity range in the subsurface is very low (400 m/s – 1800 m/s). From geotechnical viewpoint, this is indicative of loose and very weak materials. Even the velocity range, 1200 m/s to 1800 m/s, of the bottom horizon, where the tunnel passes through, cannot be attributed to sound material. The apparent increase in velocity in the bottom refractor

may only be related to the effect of overburden pressure or wetness. Hence, it is imperative to reassess the interpretations of the geoelectrical layers in light of the refraction seismic result. Because, the mean P-wave velocities of the ignimbrites of various textures and colors ranges from 2100 m/s to 3000 m/s, (e.g., Ozbek, 2013; Sowers and Boyd, 2019).

The lowest velocity range ($V_p < 700$ m/s) on the geoseismic section (Figure 7a), corresponds to the highest apparent resistivity (>350 Ω·m) on the electrical pseudo section, Figure 4a. Very often, such combination of physical signatures, low P-wave velocity and high electrical resistivity, is suggestive of loose mass, devoid of moisture. In the present case, it may reflect the low pressure (unconfined) and dry top soil, (sediments and/or highly weathered volcanic ash). On the other hand, at a comparable depth where the compressional wave velocity rises above 1200 m/s, the electrical resistivity drops below 100 Ω·m. Considering the depth to the bottom refractor (45–50 m), pressure dependent velocity rise cannot be a significant factor (e.g., Zimmer et al., 2007). It is known that the resistivity of pore fluids is a major factor that determines the bulk resistivity of porous materials. As a result, interstitial fluid is thought to be the most common cause for reduction of electrical resistivity in subsurface rocks and soils. The experimental findings of De Vita et al. (2012) details the effect of volumetric water content and soil moisture on the behavior of the electrical resistivity of pyroclastic soil.

Owing to the crystalline-solid structure of the salts, dry volcanic ash is very resistive to the flow electric current. When soaked, however, the intestinal fluid dissolve the salts and avails ionic pathway for flow of electrons, (e. g., Wardman et al., 2012). The other flaw in the earlier interpretations of the geoelectric models was the assumption made on the continuity of the lithology sequence witnessed in boreholes located about 1 km away. Summing up all the above arguments, the likely geologic formation around the tunnel alignment, which gives rise to moderate – high electrical resistivity and very low P-wave velocity, is attributed to loose and possibly wet volcanic ash.

Eventually, in agreement with the joint interpretation, the core drilling at three exploratory boreholes have not encounter a massive rock. According to the unpublished drilling report by JIANGXICO, 2018, the most dominant formations in the tunnel zone is sandy silt size volcanic ash which is thought to be deposited from lava flows during the formation of the Main Ethiopian Rift (MER), Figure 8.

4. Conclusions

This real case history demonstrates the major drawback of using a single geophysical method in engineering site assessments. The analysis in the study reveals that the gap in the interpretations of the subsurface geoelectric layers, which led to unexpected ground conditions, was due to insufficient records on the subsurface physical properties. The situation represents one of the major pitfalls that occurs when geoelectrical measurement is used as the only tool for subsurface characterization. In this typical example, the high electrically resistivity response, apparently from loose and dry volcanic ash, being mistakenly interpreted to represent a lithified (welded) rock-Ignimbrite. The premises was based on the wrong assumptions made on the continuity of the lithology sequence witnessed in boreholes at the dam-site (1 km away) to the tunnel zone. Following unexpected encounter, the application of refraction seismic as a complementary tool proves very useful in constraining the interpretation of the geoelectric models. The additional insight obtained from the P-wave velocity section is indicative of dominantly rippable (loose) mass in the subsurface. Ultimately, in a joint appraisal, it was deduced that the variations in the measured physical parameters are mainly governed by the prevalent moisture content in the volcanic ash. This was subsequently validated by the lithological log information on samples cored from the tunnel zone.

Nevertheless, the unexpected ground conditions caused considerable delay and incurred extra cost. While this study does not offer a new finding, the case history may serve as a tangible evidence for the indispensable need for an integrated approach in the applications of geophysical methods.

Declarations

Author contribution statement

Shimeles Fisseha: Conceived and designed the experiments; Performed the experiments; Analyzed and interpreted the data; Contributed reagents, materials, analysis tools or data; Wrote the paper.

Getnet Mewa; Tigistu Haile: Conceived and designed the experiments; Performed the experiments.

Funding statement

This research did not receive any specific grant from funding agencies in the public, commercial, or not-for-profit sectors.

Data availability statement

Data will be made available on request.

Declaration of interests statement

The authors declare no conflict of interest.

Additional information

No additional information is available for this paper.

Acknowledgements

The authors wish to thankfully acknowledge the Korea Rural Community Corporation (KRC) of the Republic of Korea - Ethiopia Office for facilitating the geophysical data campaigns and, as a copyright holder, availing other technical reports used for this manuscript. The authors acknowledge the SRTM30 data source: https://topex.ucsd.edu/cgi-bin/get_srtm30.cgi of Scripps Institution of Oceanography, University of California San Diego. The authors also wish to thank colleagues and anonymous reviewers for their constructive comments.

References

Agostini, A., Bonini, M., Corti, G., Sani, F., Manetti, P., 2011. Distribution of Quaternary Deformation in the central Main Ethiopian Rift, East Africa. Tectonics, 30, TC4010.

Alula, D., Boccaletti, M., Getaneh, A., Mazzuoli, R., Tortorici, L., Trua, T., 1992. Geological map of the Nazret-Dera region (main Ethiopian rift), scale 1:50,000. In: Min. degli Esteri, Cons. Naz. delle Ric., SELCA, Florence, Italy.

Becker, J.J., Sandwell, D.T., Smith, W.H.F., Braud, J., Binder, B., Depner, J., Fabre, D., Factor, J., Ingalls, S., Kim, S.-H., Ladner, R., Marks, K., Nelson, S., Pharaoh, A., Trimmer, R., Von Rosenberg, J., Wallace, G., Weatherall, P., 2009. Global bathymetry and elevation data at 30 arc seconds resolution: SRTM30_PLUS. Mar. Geodes. 32 (4), 355–371.

Biggs, J., Bastow, I.D., Keir, D., Lewi, E., 2011. Pulses of Deformation Reveal Frequently Recurring Shallow Magmatic Activity beneath the Main Ethiopian Rift. Geochemistry, Geophysics, Geosystems 12: Q0AB10.

Bonini, M., Corti, G., Innocenti, F., Manetti, P., Mazzarini, F., Abebe, T., Pecskay, Z., 2005. Evolution of the Main Ethiopian Rift in the frame of Afar and Kenya rifts propagation. Tectonics 24 (1), 1–21.

Carcione, J.M., Bjørn, U., Nordskag, J.I., 2007. Cross-property relations between electrical conductivity and the seismic velocity of rocks. Geophysics 72 (5), E193–E204.

Corti, G., 2009. Continental rift evolution: from rift initiation to incipient break-up in the Main Ethiopian Rift, East Africa. Earth Sci. Rev. 96 (1-2), 1–53.

Corti, G., Molin, P., Sembroni, A., Bastow, I.D., Keir, D., 2018. Control of pre-rift lithospheric structure on the architecture and evolution of continental rifts: insights from the Main Ethiopian Rift, East Africa. Tectonics 37, 477–496.

Corti, G., Sani, F., Florio, A.A., Greenfield, T., Keir, D., Erbello, A., Muluneh, A.A., Ayele, A., 2020. Tectonics of the Asela-Langano margin, main Ethiopian rift (East Africa). Tectonics 39 e2020TC006075.

Dahlin, T., Zhou, B., 2004. A numerical comparison of 2D resistivity imaging using ten electrode arrays. Geophys. Prospect. 52 (5), 379–398.

De Groot-Hedlin, C., Constable, S., 1990. Occam's inversion to generate smooth, two-dimensional models form magnetotelluric data. Geophysics 55, 1613–1624.

De Pasquale, G., Linde, N., Greenwood, A., 2019. Joint probabilistic inversion of DC resistivity and seismic refraction data applied to bedrock/regolith interface delineation. J. Appl. Geophys. 170, 103839.
De Vita, P., Di Maio, R., Piegari, E., 2012. A study of the correlation between electrical resistivity and matric suction for unsaturated ash-fall pyroclastic soils in the Campania region (southern Italy). Environ. Earth Sci. 67 (3), 787.
Edwards, L.S., 1977. A modified pseudosection for resistivity and induced polarization. Geophysics 42, 1020–1036.
Geology of Dodota irrigation project site, 2015. Unpublished report on the geology of Dodota irrigation project area. In: Korea Rural Community Corporation (KRC) Project Office, Addis Ababa, Ethiopia.
JIANGXICO WATER AND HYDROPOWER CONSTRUCTION co. LTD, 2018. Dodota irrigation project. In: Final Report on Core Drilling along at the Irrigation Intake Tunnel Section, from 1+100 to 1+600, Addis Ababa, Ethiopia.
Loke, M.H., 2002. RES2DINV Ver. 3.54. Rapid 2-D Resistivity and IP Inversion Using the Least Square Method. Geotomo Software.
Loke, M.H., Barker, R.D., 1996. Rapid least-squares inversion of apparent resistivity pseudosections by a quasi-Newton method. Geophys. Prospect. 44, 131–152.
Mavko, G., Mukerji, T., Dvorkin, J., 2009. The Rock Physics Handbook: Tools for Seismic Analysis of Porous, second ed. Media Cambridge University Press, pp. 266–386.
Meju, M.A., Gallardo, L.A., Mohamed, A.K., 2003. Evidence for correlation of electrical resistivity and seismic velocity in heterogeneous near-surface materials. Geophys. Res. Lett. 30 (7), 1373.
Ozbek, A., 2013. Investigation of the effects of wetting–drying and freezing–thawing cycles on some physical and mechanical properties of selected ignimbrites. Bull. Eng. Geol. Environ.
Pazzi, Veronica, Morelli, Stefano, Fanti, Riccardo, 2019. A review of the advantages and limitations of geophysical investigations in Landslide studies. Int. J. Geophys. 2019, 2983087.
SABA ENGINEERING PLC, 2015. DODOTA IRRIGATION PROJECT, Final Report on Geotechnical Core Drilling at the Keletam Dam Site, Addis Ababa, Ethiopia.
Sowers, T., Boyd, O.S., 2019. Petrologic and mineral Physics Database for Use with the U.S. Geological Survey National Crustal Model: U.S. Geological Survey Open-File Report 2019–1035, p. 17.
Telford, W.M., Geldart, L.P., Sheriff, R.E., Keys, 1990. Applied Geophysics. Cambridge University Press, pp. 632–700.
Vander Velpen, B.P.A., 2004. WinRESIST Version 1.0. Resistivity Sounding Interpretation Software. M.Sc. Research Project. ITC, Delft, the Netherlands.
Varnavina, A.V., Khamzin, A.K., Kidanu, S.T., Anderson, N.L., 2019. Geophysical site assessment in karst terrain: a case study from southwestern Missouri. J. Appl. Geophys. 170, 103838.
Vinciguerra, S., Trovato, C., Meredith, P.G., Benson, P.M., Troise, C., de Natale, G., 2006. Understanding the seismic velocity structure of Campi Flegrei Caldera (Italy): from the laboratory to the field scale. Pure Appl. Geophys. 163, 2205–2221.
Wardman, J.B., Wilson, T.M., Bodger, P.S., Cole, J.W., Johnston, D.M., 2012. Investigating the electrical conductivity of volcanic ash and its effect on HV power systems. Phys. Chem. Earth Parts A/B/C 45–46, 128–145.
Zimmer, M.A., Prasad, M., Mavko, G., Nur, A., 2007. Seismic velocities of unconsolidated sands: Part 1- Pressure trends from 0.1 to 20 MPa. Geophysics 72, 1.